

IEEE JOURNAL OF SELECTED TOPICS IN APPLIED EARTH OBSERVATIONS AND REMOTE SENSING

A PUBLICATION OF THE IEEE GEOSCIENCE AND REMOTE SENSING SOCIETY
AND THE IEEE COMMITTEE ON EARTH OBSERVATIONS



AUGUST 2016

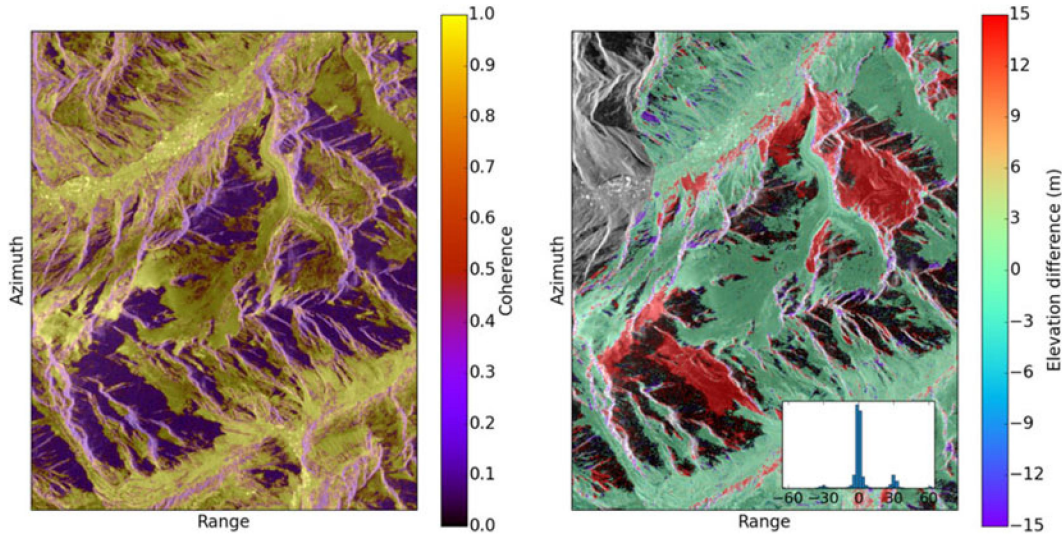
VOLUME 9

NUMBER 8

IJSTHZ

(ISSN 1939-1404)

SPECIAL ISSUE ON ANALYSIS AND APPLICATIONS OF MULTITEMPORAL DATA



Interferometric coherence (left) and elevation difference with Pléiades 2013 (right) for the TDX pair 2012/05/13 ($\text{HoA} = 30.3 \text{ m}$) unwrapped with SRTM as a reference, in the radar geometry. Inset shows the histogram of the elevation differences. Background is the amplitude image: dark regions are areas of shadow, very bright regions are areas of layover. Areas disconnected from the rest of the image due to shadow/layover (low coherence) tend to have more unwrapping errors (in purple/red in the right image). For more information, please see “Elevation Changes Inferred From TanDEM-X Data Over the Mont-Blanc Area: Impact of the X-Band Interferometric Bias,” by Dehecq, *et al.*, which begins on p. 3870.

IEEE JOURNAL OF SELECTED TOPICS IN APPLIED EARTH OBSERVATIONS AND REMOTE SENSING

A PUBLICATION OF THE IEEE GEOSCIENCE AND REMOTE SENSING SOCIETY
AND THE IEEE COMMITTEE ON EARTH OBSERVATIONS



AUGUST 2016

VOLUME 9

NUMBER 8

IJSTHZ

(ISSN 1939-1404)

SPECIAL ISSUE ON ANALYSIS AND APPLICATIONS OF MULTITEMPORAL DATA

GUEST EDITORIAL

Foreword to the Special Issue on Analysis of Multitemporal Data and Applications	3356
..... <i>E. Trouvé, G. Mercier, M. Fauvel, L. Bruzzone, and Y. Ban</i>	

Change Detection

A Relative Density Ratio-Based Framework for Detection of Land Cover Changes in MODIS NDVI Time Series	3359
..... <i>A. Anees, J. Aryal, M. M. O'Reilly, and T. J. Gale</i>	
A Simple Transformation for Visualizing Non-seasonal Landscape Change From Dense Time Series of Satellite Data	3372
..... <i>J. N. Hird, G. Castilla, G. J. McDermid, and I. T. Bueno</i>	
Learning Relationship for Very High Resolution Image Change Detection	3384
..... <i>C. Huo, K. Chen, K. Ding, Z. Zhou, and C. Pan</i>	
Discriminative Random Fields Based on Maximum Entropy Principle for Semisupervised SAR Image Change Detection	3395
..... <i>L. An, M. Li, P. Zhang, Y. Wu, L. Jia, and W. Song</i>	
Remote-Sensing Image Change Detection With Fusion of Multiple Wavelet Kernels	3405
..... <i>L. Jia, M. Li, P. Zhang, Y. Wu, L. An, and W. Song</i>	
Multitemporal SAR Image Decomposition into Strong Scatterers, Background, and Speckle	3419
..... <i>S. Lobry, L. Denis, and F. Tupin</i>	
Building Change Detection Using High Resolution Remotely Sensed Data and GIS	3430
..... <i>N. Sofina and M. Ehlers</i>	
Automatic Change Detection in High-Resolution Remote Sensing Images by Using a Multiple Classifier System and Spectral-Spatial Features	3439
..... <i>K. Tan, X. Jin, A. Plaza, X. Wang, L. Xiao, and P. Du</i>	
SAR Images Change Detection Based on Spatial Coding and Nonlocal Similarity Pooling	3452
..... <i>S. Wang, L. Jiao, and S. Yang</i>	
Individual Tree Crown Modeling and Change Detection From Airborne Lidar Data	3467
..... <i>W. Xiao, S. Xu, S. O. Elberink, and G. Vosselman</i>	
Change Detection Based on Conditional Random Field With Region Connection Constraints in High-Resolution Remote Sensing Images	3478
..... <i>L. Zhou, G. Cao, Y. Li, and Y. Shang</i>	

(Contents Continued on Page 3354)

<i>Estimation</i>		
Extending Airborne Lidar-Derived Estimates of Forest Canopy Cover and Height Over Large Areas Using kNN With Landsat Time Series Data	O. S. Ahmed, S. E. Franklin, M. A. Wulder, and J. C. White	3489
Analysis of Polarimetric Radar Data and Soil Moisture From Aquarius: Towards a Regression-Based Soil Moisture Estimation Algorithm	M. S. Burgin and J. J. van Zyl	3497
Equatorial Forests Display Distinct Trends in Phenological Variation: A Time-Series Analysis of Vegetation Index Data from Three Continents	E. A. Cherrington, N. Barbier, P. Ploton, G. Vincent, D. Sabatier, U. Berger, and R. Pélassier	3505
Contribution to Real-Time Estimation of Crop Phenological States in a Dynamical Framework Based on NDVI Time Series: Data Fusion With SAR and Temperature	C. De Bernardis, F. Vicente-Guijalba, T. Martinez-Marin, and J. M. Lopez-Sanchez	3512
Satellite Gravimetric Estimation of Groundwater Storage Variations Over Indus Basin in Pakistan	N. Iqbal, F. Hossain, H. Lee, and G. Akhter	3524
Assessment of the Evolution of Nitrate Deposition Using Remote Sensing Data Over the Yangtze River Delta, China	M. Cheng, Z. Guo, H. Dang, Y. He, G. Zhi, J. Chen, Y. Zhang, W. Zhang, and F. Meng	3535
Prediction of Land-Surface Temperatures of Jaipur City Using Linear Time Series Model	A. Mathew, S. Sreekumar, S. Khandelwal, N. Kaul, and R. Kumar	3546
Data Uncertainty in an Improved Bayesian Network and Evaluations of the Credibility of the Retrieved Multitemporal High-Spatial-Resolution Leaf Area Index (LAI)	W. Han and Y. Qu	3553
A Functional Form for the Diurnal Variation of Lake Surface Temperature on Lake Hartwell, Northwestern South Carolina	J. L. Hodges, J. R. Saylor, and N. B. Kaye	3564
Using Geoindicators to Prioritize Regional Wetland Locations for Flood Attenuation in Manitoba's Red River Basin	S. Fraser and J. L. Storie	3578
An Effective Compound Algorithm for Reconstructing MODIS NDVI Time Series Data and Its Validation Based on Ground Measurements	L. Geng, M. Ma, and H. Wang	3588
Estimating Site Index From Short-Term TanDEM-X Canopy Height Models	H. J. Persson and J. E. S. Fransson	3598
Exploring the Validity of the Long-Term Data Record V4 Database for Land Surface Monitoring	J. A. Sobrino and Y. Julien	3607
<i>Clouds</i>		
Cloud Removal in Image Time Series Through Sparse Reconstruction From Random Measurements	D. Cerra, J. Bieniarz, F. Beyer, J. Tian, R. Müller, T. Jarmer, and P. Reinartz	3615
Patch Matching-Based Multitemporal Group Sparse Representation for the Missing Information Reconstruction of Remote-Sensing Images	X. Li, H. Shen, H. Li, and L. Zhang	3629
<i>Classification/Segmentation/Mapping/Detection</i>		
Spatio–Temporal Clustering and Active Learning for Change Classification in Satellite Image Time Series	N. Débonnaire, A. Stumpf, and A. Puissant	3642
Synergy Between LiDAR, RADARSAT-2, and Spot-5 Images for the Detection and Mapping of Wetland Vegetation in the Danube Delta	S. Niculescu, C. Lardeux, I. Grigoras, J. Hanganu, and L. David	3651
Error Sources in Deforestation Detection Using BFAST Monitor on Landsat Time Series Across Three Tropical Sites	M. Schultz, J. Verbesselt, V. Avitabile, C. Souza, and M. Herold	3667
Multitemporal Analysis of High-Spatial-Resolution Optical Satellite Imagery for Mangrove Species Mapping in Bali, Indonesia	G. Viennois, C. Proisy, J.-B. Féret, J. Prosperi, F. Sidik, Suhardjono, R. Rahmania, N. Longépé, O. Germain, and P. Gaspar	3680
Monitoring of Agricultural Grasslands With Time Series of X-Band Repeat-Pass Interferometric SAR	K. Zalite, O. Antropov, J. Praks, K. Voormansik, and M. Noorma	3687
Regional Glacier Mapping Using Optical Satellite Data Time Series	S. H. Winsvold, A. Kääb, and C. Nuth	3698
Efficiency Assessment of Multitemporal C-Band Radarsat-2 Intensity and Landsat-8 Surface Reflectance Satellite Imagery for Crop Classification in Ukraine	S. Skakun, N. Kussul, A. Y. Shelestov, M. Lavreniuk, and O. Kussul	3712

A Spatio-Temporal Data-Mining Approach for Identification of Potential Fishing Zones Based on Oceanographic Characteristics in the Eastern Indian Ocean	D. Fitrianah, A. N. Hidayanto, J. L. Gaol, H. Fahmi, and A. M. Arymurthy	3720
A Time-Weighted Dynamic Time Warping Method for Land-Use and Land-Cover Mapping	V. Maus, G. Câmara, R. Cartaxo, A. Sanchez, F. M. Ramos, and G. R. de Queiroz	3729
<i>Urban</i>		
Urban Areas Enhancement in Multitemporal SAR RGB Images Using Adaptive Coherence Window and Texture Information	D. Amitrano, V. Belfiore, F. Cecinati, G. Di Martino, A. Iodice, P.-P. Mathieu, S. Medagli, D. Poreh, D. Riccio, and G. Ruello	3740
Viewing Global Megacities Through MODIS 4- μm Radiance: Effects of Time of Year, Latitude, Land Cover, and View Zenith Angle	M. Tomaszewska, V. Kovalskyy, C. Small, and G. M. Henebry	3753
The Interferometric Use of Radar Sensors for the Urban Monitoring of Structural Vibrations and Surface Displacements	A. Montuori, G. Luzi, C. Bignami, I. Gaudiosi, S. Stramondo, M. Crosetto, and M. F. Buongiorno	3761
Simulation-Based Building Change Detection From Multiangle SAR Images and Digital Surface Models	J. Tao and S. Auer	3777
Building Collapse Assessment in Urban Areas Using Texture Information From Postevent SAR Data	W. Sun, L. Shi, J. Yang, and P. Li	3792
<i>SAR Processing</i>		
A Temporal Estimation of Entropy and Its Comparison With Spatial Estimations on PolSAR Images	F. Weissgerber, E. Colin-Koeniguer, N. Trouvé, and J.-M. Nicolas	3809
Application of the Variational-Mode Decomposition for Seismic Time-frequency Analysis	Y.-J. Xue, J.-X. Cao, D.-X. Wang, H.-K. Du, and Y. Yao	3821
TOPS Time Series Performance Assessment With TerraSAR-X Data	M. Nannini, P. Prats-Iraola, F. De Zan, and D. Geudtner	3832
Active Microwave Scattering Signature of Snowpack—Continuous Multiyear SnowScat Observation Experiments	C.-C. Lin, B. Rommen, N. Flouri, D. Schüttemeyer, M. W. J. Davidson, M. Kern, A. Kontu, J. Lemmettyinen, J. Pulliainen, A. Wiesmann, C. L. Werner, C. Mätzler, M. Schneebeli, M. Proksch, and T. Nagler	3849
Elevation Changes Inferred From TanDEM-X Data Over the Mont-Blanc Area: Impact of the X-Band Interferometric Bias	A. Dehecq, R. Millan, E. Berthier, N. Gourmelen, E. Trouvé, and V. Vionnet	3870
A Minimum Acceleration Approach for the Retrieval of Multiplatform InSAR Deformation Time Series	A. Pepe, G. Solaro, F. Cal, and C. Dema	3883
